

# Whispering gallery modes and other cavity modes for perfect backscattering and blazing

E. Popov,\* D. Maystre, and G. Tayeb

*Institut Fresnel, Aix-Marseille Université, CNRS UMR 6133, Domaine Universitaire de St. Jerome,  
13397 Marseille CEDEX 20, France*

\*Corresponding author: e.popov@fresnel.fr

Received March 23, 2010; accepted May 2, 2010;  
posted May 6, 2010 (Doc. ID 125890); published June 9, 2010

We demonstrate the possibility to obtain perfect blazing both in Littrow and off-Littrow mountings using diffractive systems consisting of a plane metallic substrate and dielectric structures that can support cavity modes. The resonances are located at a relatively large distance between the metal and the dielectric structure, a condition that prevents the resonance increase of absorption. The high efficiency can be obtained in transverse electric or transverse magnetic polarization and at high incident angles. When cylindrical rods with circular cross-sections are used, the so-called whispering gallery modes can be used to provide the resonances, necessary for the blazing. © 2010 Optical Society of America  
OCIS codes: 050.0050, 230.1950, 050.5745.

## 1. INTRODUCTION

It is well known that resonant phenomena play an important role in optics (and in nature, in general). In particular, Bloch modes in periodic (or almost periodic) systems can create forbidden gaps for the corresponding waves. Typical examples are the electronic forbidden gaps in crystal structures and the photonic bandgaps in photonic crystals. Most research dedicated to photonic crystals considers subwavelength cells that do not create diffracted propagating waves. However, periodic structures known as diffraction gratings were widely studied and used in optics and optical engineering long before the term photonic crystal emerged.

While it is thought that the first use of diffraction gratings was described by Young [1], it is not well known that the first recorded observation of light diffraction by a periodic structure (nowadays known as a grating having two-dimensional periodicity) was made by Francis Hopkinson, who was George Washington's first Secretary of the Navy and one of the signers of the Declaration of Independence. In 1785 he observed a phenomenon of multiple images created when the light of a distant street lamp passed through a fine French silk handkerchief, a discovery explained and used by his friend the astronomer Rittenhouse [2]. An interested reader can find a summary of the fascinating history of diffraction grating studies in [3].

Another fact that is generally ignored is the possibility to use the nowadays widely studied photonic bandgaps in order to create high-efficiency diffraction gratings. The idea is simple: if the propagation of light is forbidden in all but one direction, and if this direction is chosen to occur in a propagating non-specular diffraction order, it will bring all the incident light, thus having 100% diffraction efficiency [4,5]. If the gap is forbidden for unpolarized light, it can be used to create perfect blazing for arbitrary polarization [5].

About 25 years ago we showed that a simple periodic structure with one-dimensional periodicity capable of supporting some kind of electromagnetic resonances can have 100% reflectivity close to the resonance, even if it is otherwise almost transparent. At that time we used the excitation of guided modes in corrugated dielectric waveguides [6], which allowed for the possibility to construct narrowband filters working in reflection. However, for quite a long time, their applications have been limited by their resonant nature—the narrower the spectral band, the tighter the tolerance of the collimation of the light beam. It took more than 10 years and the knowledge of bandgap properties to increase the angular tolerances by another interaction (between counter-propagating modes [7]) in order to pass from theory to applications.

Another possibility of reducing the angular dependence of the reflectivity maximum is to use resonances that are less sensitive angularly, for example, cavity resonances. Periodical arrangement of optical fibers with subwavelength periods can be characterized by narrow spectral lines in reflection, while keeping the angular resonances reasonable for practical use [8]. The idea is to use the so-called whispering gallery modes, discovered by Rayleigh in acoustics [9,10]. They represent waves propagating at the oval (circular, in particular) surface of a cylindrical object and confined inside by an almost total internal reflection. There are many papers devoted to whispering modes (WsM) in optical fibers, although much less than in dielectric spheres. Initially, the interest was motivated by bending and coupling losses in fibers [11–18]. More recently, the use of WsM for guiding of light has been proposed [19–21]. Although the WsM are lossy (radiative), they can guide light along a long chain of aligned fibers [22], because the losses are small.

The aim of this paper is to study the possibility of using cavity resonances in order to create bandgaps that can be used for constructing diffraction gratings presenting per-

fect blazing in a single non-specular diffracted order. First, we use the WsM in fibers. Based on that analysis, we then study the cavity modes in rectangular structures that can be assembled much easier than the set of equidistant fibers.

The calculations in this paper have been obtained using three different rigorous electromagnetic methods. The first method called scattering matrix method is specific to finite-number line of cylinders [23] and is used for the calculations of poles of the modes of single cylinders. Most of the calculations for the periodic infinite set of cylinders with or without a substrate, as well as later for the lamellar gratings, are made using the differential method [24]. In order to check the validity of the results, we used a code based on the integral method [25].

## 2. WHISPERING GALLERY MODES, TOTAL LIGHT REFLECTION, AND PERFECT BLAZING

Let us consider an infinite set (period  $d=1 \mu\text{m}$ ) of circular fibers with an optical index of 3.45 at wavelength  $\lambda = 1.55 \mu\text{m}$ , suspended in air (see the inset of Fig. 1) and illuminated in transverse electric (TE, electric field vector parallel to the fiber axis) polarization at normal incidence. Figure 1 presents the dependence of the reflectivity as a function of the cylinder radius  $r$ . As can be observed, close to certain radii, there are regions with 100% reflectivity. We shall see that these values of the radius correspond to excitation of gallery modes inside the dielectric cylinders. These modes present electromagnetic resonances characterized by poles of the scattering matrix. Assuming symmetry properties (which is the case here), one can expect reading 100% maxima in the reflectance and transmittance of the system [6], which explains why a system with a relatively low optical density (for example, cylinder diameter over the period ratio of 0.25 for the first maximum) can reflect 100% of the incident light.

The map of the amplitude of the electric field  $A$  within a single period is presented in Fig. 2 for four values of  $r$ , corresponding to the maxima in Fig. 1. For a lossless structure and 100% reflection, it is possible to demonstrate that the electric field  $E$  can be represented in the

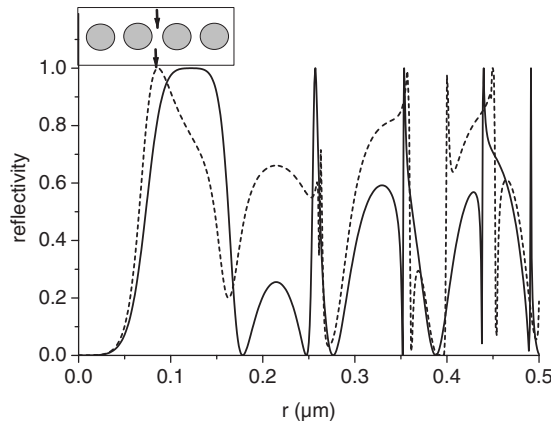


Fig. 1. Solid curve: reflectivity of a set of dielectric circular cylinders (shown in the inset) having period  $d=1 \mu\text{m}$  with refractive index of 3.45 at wavelength of  $1.55 \mu\text{m}$ , illuminated normally in TE polarization. Dashed curve:  $20^\circ$  incidence.

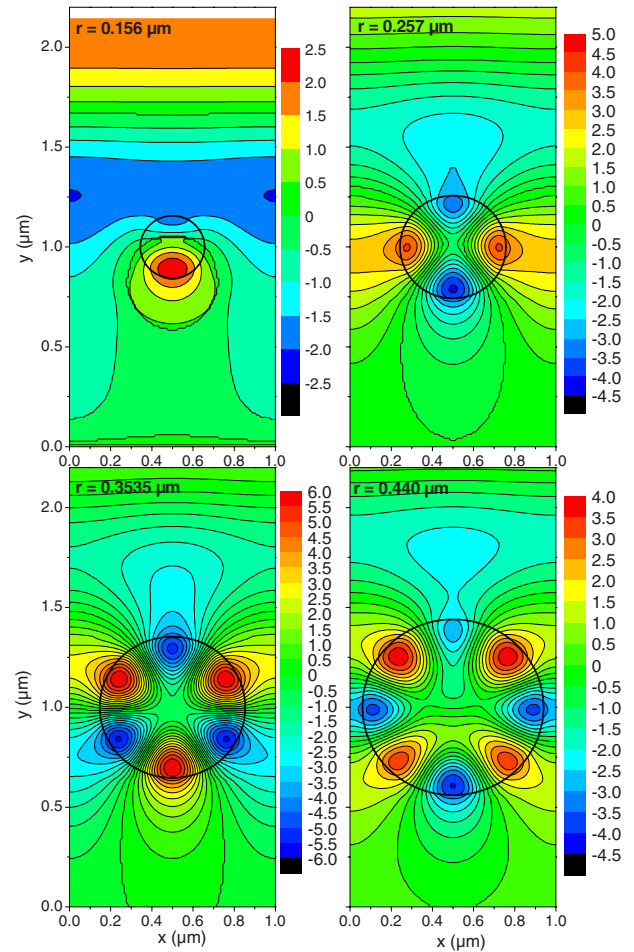


Fig. 2. (Color online) Map of the electric field amplitude in a single grating period ( $d=1 \mu\text{m}$ ), with the cylinder center positioned at  $x=0.5 \mu\text{m}$  and  $y=1 \mu\text{m}$ . The heavy circles represent the cylinder-air interface. The radius for each figure is given inside.

form of a real amplitude  $A$  multiplied by a phase factor, which does not depend on the position,  $E(x,y) = A(x,y)\exp(i\varphi)$ . This fact can be used to represent the map of  $A$  instead of the map of the modulus of  $E$  and thus to preserve the information about the sign of  $A$ , as observed in the figure.

The gallery modes are clearly visible, with positive- and negative-value maxima of the field alternating along the cylinder surface and the number of maxima (corresponding to twice the mode number) growing with the cylinder radius. It is interesting to notice that the field is strongly localized near the interface, which means that there is relatively weak coupling between the cylinders in the chain. The higher the mode number, the sharper the maxima, which in fact leads to stronger dependence on the radius as seen in Fig. 1 when moving from left to right.

The normal incidence determines that the field must be symmetrical with respect to the vertical plane, which determines the symmetry of the field maps. When we chose another incident direction, the symmetry disappears and some of the maxima get split in two, but until there is only the specular order that can propagate, the conditions described in [6] hold and the maxima in reflection can reach 100%. When the angle of incidence exceeds  $33.36^\circ$ ,

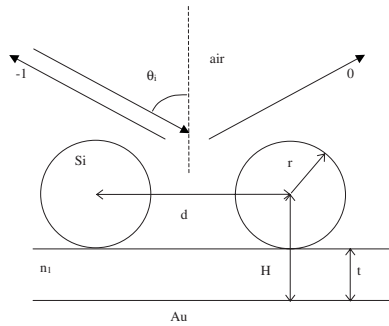


Fig. 3. Schematic presentation of the system under study with the notations.

the  $-1$ st diffracted order starts to propagate (with  $\lambda/d = 1.55$ ) so that there are four propagating diffracted orders. The diffracted energy is redistributed unevenly among them, and it is difficult to expect 100% efficiency in one of them, because the grating is not blazed. However, we can reduce the number of propagating orders by adding a reflecting substrate as shown schematically in Fig. 3, where a dielectric layer is added to support the grating.

Let us at first consider the system already studied in the previous figure, but used in  $-1$ st order Littrow mount, i.e., as in Fig. 3 but with  $n_1 = 1$ . Figure 4(a) presents the diffraction efficiencies of orders  $-1$  and  $0$  in reflection as functions of  $r$  for  $d = 1 \mu\text{m}$ ,  $H = 1 \mu\text{m}$ ,  $\lambda = 1.55 \mu\text{m}$ , angle of incidence of  $50.8^\circ$  (which corresponds to Littrow conditions for order  $-1$ ) in TE polarization, and without the metallic substrate. The same depen-

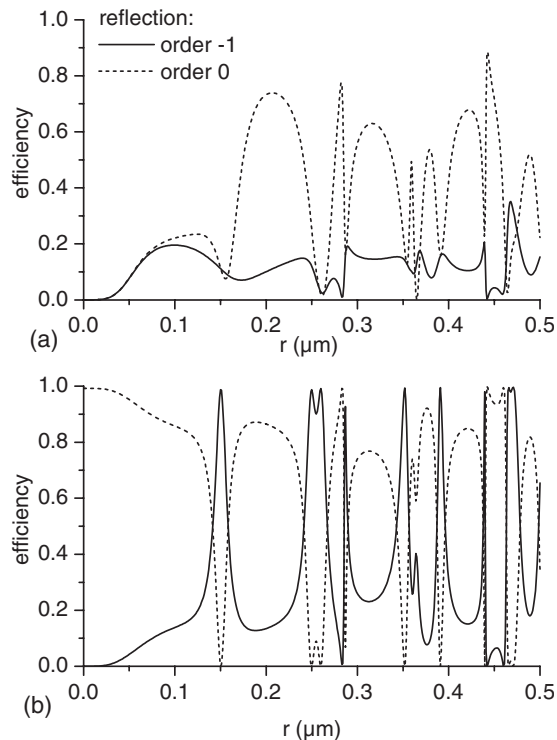


Fig. 4. Diffraction efficiency in the  $-1$ st and zeroth reflection orders as a function of the rod radius of the structure presented in Fig. 3 with  $d = 1 \mu\text{m}$ ,  $H = 1 \mu\text{m}$ ,  $\lambda = 1.55 \mu\text{m}$ ,  $n_1 = 1$ , and angle of incidence of  $50.8^\circ$  in TE polarization. (a) Without the substrate, (b) with gold substrate.

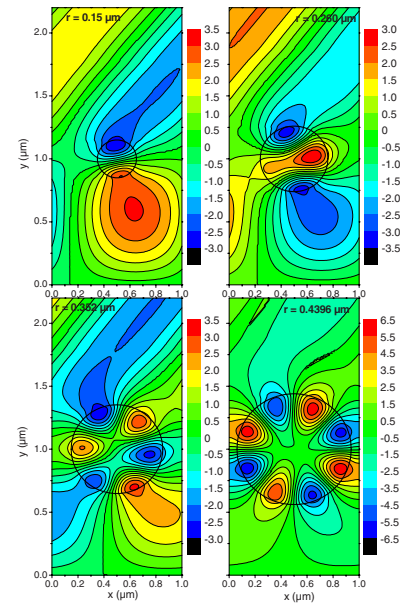


Fig. 5. (Color online) Same as in Fig. 2 but for gold substrate and  $50.8^\circ$  angle of incidence.

dences when adding the substrate (complex refractive index  $0.36 + i10.4$ ) are given in Fig. 4(b).

Without the reflecting lower surface, the efficiencies oscillate rapidly with the radius, more rapidly than in Fig. 1, but never reach 100% (but some of them exceed 99.6%), which can be expected as discussed above. However, similarly to Fig. 1, sharp oscillations appear close to the radius values given in Fig. 2, with the difference being larger for smaller rods, when the gallery modes are less confined and more strongly coupled in-between the rods, and thus more dependent of the incident conditions. With the metallic substrate, some of the maxima reach almost 100%. Due to the finite conductivity of the substrate, there are some absorption losses, but when we are using infinitely conducting substrate, the maxima reach 100%. As can be expected, the field maps at the  $-1$ st order efficiency maxima given in Fig. 5 are similar to those in Fig. 2 at slightly different radii, because the gallery mode confinement diminishes the coupling between the different rods, and also between the rods and the conducting substrate.

### 3. PHENOMENOLOGICAL APPROACH TO THE EXPLANATION OF THE PERFECT BLAZING

Let us consider a perfectly conducting substrate and a grating suspended in air ( $n_1 = 1$ ; see Fig. 3) with both horizontal (with respect to the  $Oyz$  plane) and vertical (with respect to the  $Oxz$  plane) symmetries. Let us consider the far-field region, where all the evanescent diffraction orders have disappeared. In TE polarization, the electric field above the grating can be represented as a sum of three propagating waves: the incident wave with amplitude  $a_0$ , the reflected wave with amplitude  $b_0$ , and the diffracted wave with amplitude  $b_{-1}$ . We have added another incident wave with amplitude  $a_{-1}$ , necessary further on

when considering the scattering ( $S$ ) matrix of the system. Now we assume that  $a_{-1}=0$  so that

$$E_z = a_0 \exp(i\alpha x - i\beta y) + b_0 \exp(i\alpha x + i\beta y) + b_{-1} \exp(-i\alpha x + i\beta y), \quad y \geq R, \quad (1)$$

where

$$\alpha = k_0 \sin \theta_i, \quad (2)$$

$$\beta = \sqrt{k_0^2 - \alpha^2},$$

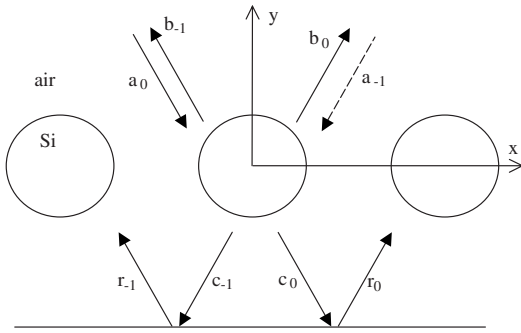
with  $k_0 = 2\pi/\lambda$ .

Assuming that the distance between the dielectric structure and the metallic substrate is sufficiently large to neglect the evanescent orders, there are only four plane waves close to the metallic surface as shown in Fig. 6(a) so that the electric field is written in the form

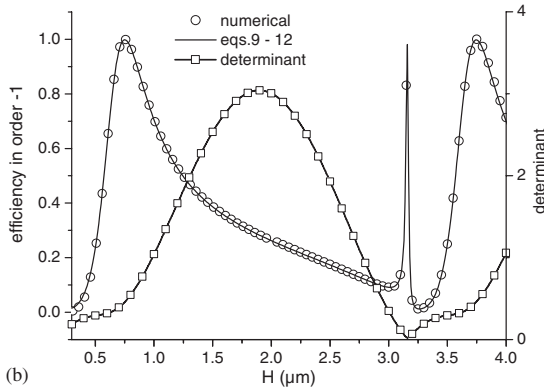
$$E_z = c_0 \exp(i\alpha x - i\beta y) + c_{-1} \exp(-i\alpha x - i\beta y) + r_0 \exp(i\alpha x + i\beta y) + r_{-1} \exp(-i\alpha x + i\beta y), \quad y \leq -R. \quad (3)$$

The electric field is null in the substrate so that

$$r_0 = -c_0 \exp(2i\beta H),$$



(a)



(b)

Fig. 6. (a) Schematic representation of the dielectric grid and propagating orders. (b) Diffraction efficiency in order  $-1$  and modulus of the determinant of the linear system, Eq. (10), as a function of the distance  $H$  of the rod centers from the perfectly conducting metallic surface of the system, presented in Fig. 3 with  $n_1=1$ ,  $d=0.80234 \mu\text{m}$ ,  $r=0.30825 \mu\text{m}$ ,  $\lambda=1.55 \mu\text{m}$ ,  $\theta_i=75^\circ$ , and Si refractive index  $n=3.45$ .

$$r_{-1} = -c_{-1} \exp(2i\beta H), \quad (4)$$

where  $H=t+r$  is the distance from the substrate to the center of symmetry of the grating.

If we eliminate the substrate, the amplitudes  $r_0$  and  $r_{-1}$  become null. The amplitudes of the field scattered by the grating are proportional to the incident amplitude,

$$b_0 = R a_0, \quad b_{-1} = D_r a_0, \quad (5)$$

$$c_0 = T a_0, \quad c_{-1} = D_t a_0,$$

where  $R$  and  $T$  are the reflection and transmission coefficients, respectively, and  $D_r$  and  $D_t$  are the diffraction coefficients in reflection and in transmission, respectively, without the substrate.

However, if the substrate is eliminated, the incident wave can propagate upward, and we can consider the case when the only incident wave is the wave with amplitude  $r_0$ . Due to the symmetry of the grating structure, it is easy to see that in that case, if  $a_0=r_{-1}=0$ ,

$$b_0 = T r_0, \quad b_{-1} = D_t r_0, \quad (6)$$

$$c_0 = R r_0, \quad c_{-1} = D_r r_0.$$

Furthermore, if  $a_0=r_0=0$  and the only incident wave is the one with amplitude  $r_{-1}$ , we get the relations

$$b_0 = D_t r_{-1}, \quad b_{-1} = T r_{-1}, \quad (7)$$

$$c_0 = D_r r_{-1}, \quad c_{-1} = R r_{-1}.$$

Going back to the case with reflecting grid so that

$$c_0 = R r_0 + D_r r_{-1} + T a_0, \quad (8)$$

$$c_{-1} = D_r r_0 + R r_{-1} + D_t a_0,$$

$$b_0 = T r_0 + D_t r_{-1} + R a_0, \quad (9)$$

$$b_{-1} = D_t r_0 + T r_{-1} + D_r a_0.$$

Combining Eqs. (4) and (8) produces a linear system of two equations for  $r_0$  and  $r_{-1}$ , with a determinant  $\Delta$  equal to

$$\Delta = [\exp(-2i\beta H) - R]^2 - D_r^2, \quad (10)$$

with the following solutions:

$$r_0 = \{D_r D_t - T[R + \exp(-2i\beta H)]\} \frac{a_0}{\Delta},$$

$$r_{-1} = \{D_r T - D_t[R + \exp(-2i\beta H)]\} \frac{a_0}{\Delta}. \quad (11)$$

These formulas permit us immediately to obtain the amplitudes scattered in the cladding by using Eq. (9).

Let us consider the following set of parameters with all lengths in micrometers:  $d=0.80234$ ,  $r=0.30825$ ,  $\lambda=1.55$ ,  $\theta_i=75^\circ$ , and Si refractive index  $n=3.45$ . The numerical values of the different coefficients without substrate, ob-

tained using the rigorous electromagnetic theory that takes into account the evanescent waves, are equal to

$$\begin{aligned} D_r &= 0.413\ 76 \exp(i20.62^\circ), & R &= 0.712\ 18 \exp(i137.85^\circ), \\ D_t &= 0.455\ 74 \exp(i24.82^\circ), & T &= 0.336\ 90 \exp(-i3.81^\circ). \end{aligned} \quad (12)$$

Figure 6(b) presents the diffracted amplitude as a function of  $H$ , calculated either by using Eqs. (9)–(12) with  $\lambda = 1.55$ ,  $\theta_i = 75^\circ$  or with the rigorous electromagnetic modeling that takes into account the evanescent diffracted orders. There is practically no difference between the two approaches, which is not surprising if the distance between the grating and the reflecting surface is sufficiently large so that the evanescent waves created at the dielectric grid do not reach the metallic substrate.

It is necessary to underline that the results presented in Fig. 6 enable perfect blazing close to grazing incidence ( $75^\circ$ ), which cannot easily be obtained using other techniques. In Section 5 we will go back to that question with more realistic structures than in these theoretical considerations.

We observe in Fig. 6 several features: wide maxima and sharp anomalies. They appear periodically as functions of  $H$ , which is natural bearing in mind that the results depend on  $\exp(-2i\beta H)$  only. The sharp anomalies are due to the Fabry–Perot resonances, appearing when  $\Delta$  is equal to zero, also presented in the figure. The wide maxima can be interpreted by an interference effect between different contributions in the right-hand-sides of Eqs. (9). This interference becomes destructive into order 0 leading to blazing in order  $-1$  (maxima in the figure) or destructive in order  $-1$  (minima in the figure), enhancing the reflection.

However, this interpretation does not answer the question to know why the blazing becomes perfect, i.e., why the interference between the three contributions to  $b_0$  and  $b_{-1}$  in Eqs. (9) can completely eliminate the specular reflection. In order to answer that question, we present an analysis of the properties of the scattering matrix of the system, including both the grating structure and the perfectly conducting substrate. In that case we can consider a square matrix of size 2, which is easy to analyze. In order to introduce the scattering ( $S$ ) matrix, we consider a second wave incident on the cladding in a symmetrical direction as shown in Fig. 6(a) with a dashed arrow. Let us return to the field representation far above the grating structure [Eq. (1)], assuming two incident and two diffracted propagating waves,

$$\begin{aligned} E_z &= a_0 \exp(i\alpha x - i\beta y) + a_{-1} \exp(-i\alpha x - i\beta y) + b_0 \exp(i\alpha x \\ &\quad + i\beta y) + b_{-1} \exp(-i\alpha x + i\beta y), \end{aligned} \quad (13)$$

By definition, the  $S$  matrix links the diffracted and the incident amplitudes,

$$\begin{pmatrix} b_0 \\ b_{-1} \end{pmatrix} = \begin{pmatrix} S_{0,0} & S_{0,-1} \\ S_{-1,0} & S_{-1,-1} \end{pmatrix} \begin{pmatrix} a_0 \\ a_{-1} \end{pmatrix}. \quad (14)$$

The case of an electromagnetic resonance is characterized by a pole  $\alpha^p$  of the scattering matrix. A guided wave is a typical example, because a pole means that there could be

diffracted waves without any incident one, as it follows from Eq. (14). Usually, the pole is a pole of the coefficients of the scattering matrix, except if there is no coupling between different diffracted orders. Let us consider the reflection from  $a_0$  into  $b_0$ . If there is a single pole of  $S_{0,0}$  (existence of guided or surface wave or cavity mode), the reflectivity contains two contributions:

$$S_{0,0}(\alpha) \approx R_{\text{n.r.}} + \frac{C_r}{\alpha - \alpha^p}. \quad (15)$$

The first one,  $R_{\text{n.r.}}$ , is non-resonant and the second one is resonant, with a slowly varying coefficient  $C_r$ . In fact, these are the first two terms in the Laurent series of  $S_{0,0}$  as a function of  $\alpha$ . The two terms interfere, which can increase or decrease the reflection. By combining the two terms, we obtain another expression,

$$S_{0,0}(\alpha) \approx R_{\text{n.r.}} \frac{\alpha - \alpha_{0,0}^z}{\alpha - \alpha^p}, \quad \alpha_{0,0}^z = \alpha^p - \frac{C_r}{R_{\text{n.r.}}}. \quad (16)$$

Thus  $S_{0,0}$  must have a zero, accompanying the pole. This can be explained by the disappearance of the resonant term if the grating strength is zero so that no coupling is possible between the incident wave and the resonance. When the coupling  $C_r$  disappears, the zero coincides with the pole and only the non-resonant contribution remains in reflection.

In general, the pole is complex, because otherwise the reflection would tend to infinity for real angle of incidence and wavelength corresponding to the pole value. The zero is also complex, but for some set of optogeometrical parameters, it can become real. In that case, if  $\alpha$  is equal to  $\alpha_{0,0}^z$ ,  $S_{0,0} = 0$ , the reflection vanishes and all the non-absorbed light goes into the diffracted order.

#### 4. FEASIBLE STRUCTURES WITH CIRCULAR RODS

Let us now study more realistic structures that can be more easily fabricated than the chain of fibers suspended in air. If we consider cylindrical rods, in order to position them in equidistant order preserving some mutual distance, there is a possibility to prepare beds in the underlying dielectric layer (Fig. 3) by photolithographic technology and chemical or ion-beam etching, in order to obtain structures, presented schematically in Figs. 7(a) and 7(b). We can expect that if the contrast of the refractive index between the rods and the underlying dielectric is kept sufficiently high, there will be gallery modes. Indeed, Fig. 8(a) presents the efficiency in order  $-1$  for a structure given in Fig. 7(a) with  $n_1 = 1.5$ , with the other parameters being the same as in Fig. 5. The efficiency exhibits a behavior similar to the case with  $n_1 = 1$ . This is not surprising, as long as the gallery modes have similar field maps, which is the case at least for radius values presented in Fig. 8(b), when compared with Fig. 5.

Anyway, several differences between the cases  $n_1 = 1$  and 1.5 require special attention in view of the next analysis of rectangular rod diffraction. First, larger rods lead to stronger absorption losses [the dashed curve in Fig. 8(a) presents the total non-absorbed energy] due to

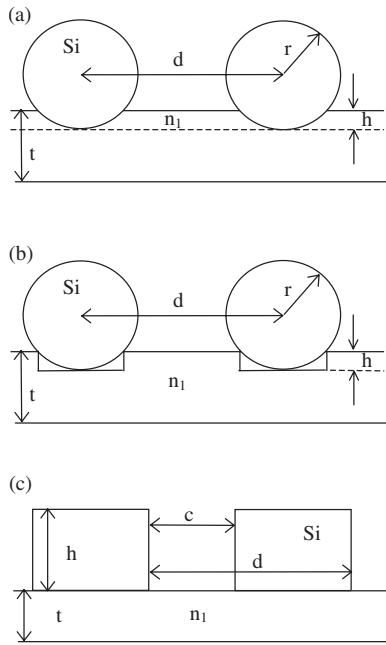


Fig. 7. Schematic presentation of different grating structures.

the stronger coupling between the gallery modes and the substrate through the dielectric layer that now is denser optically. Second, the field behavior in this layer changes [Fig. 8(b)]; it becomes stronger inside the dielectric layer, which is again expected when its optical index is higher.

### 5. CAVITY RESONANCES INSIDE RECTANGULAR RODS

Circular rods have the advantage of supporting gallery modes (although they are not whispering in the acoustic sense as in the initial study of Rayleigh [9,10]), but their fabrication with tolerances of the radius not exceeding a few nanometers is beyond the limit of the recent technology. Probably more important is the difficulty to position them equidistantly inside the prefabricated beds as sketched in Figs. 7(a) and 7(b) that will cause perturbations in the periodicity due to the variation of radii that will reduce the grating resolution and increase scatter and diffusion [3].

Much better developed is photolithography using prefabricated masks for the following wet or dry chemical or ion-beam etching that finishes with features having profiles close to lamellar or trapezoidal profile with steep facets. As long as these structures can have electromagnetic resonances leading to pole(s) and zeros of the components of the scattering matrix  $S$ , we can expect perfect blazing in Littrow mount (backscattering configuration), following the conclusions of Section 3. Figure 9(a) gives the efficiency in the  $-1$ st order for the system sketched in Fig. 7(c) as a function of the rod height for two different widths and the following parameters:  $d=1 \mu\text{m}$ ,  $\lambda=1.55 \mu\text{m}$ ,  $\theta_i=50.8^\circ$ , and  $n_1=1.5$ . The substrate is gold with a refractive index equal to  $0.36+i10.4$ , the rod index is 3.45, and the rod center is at height  $H=(t+h/2)=1 \mu\text{m}$  from the substrate. The solid curve corresponds to  $c=0.7 \mu\text{m}$  (rod width of  $0.3 \mu\text{m}$ ); the dashed curve to

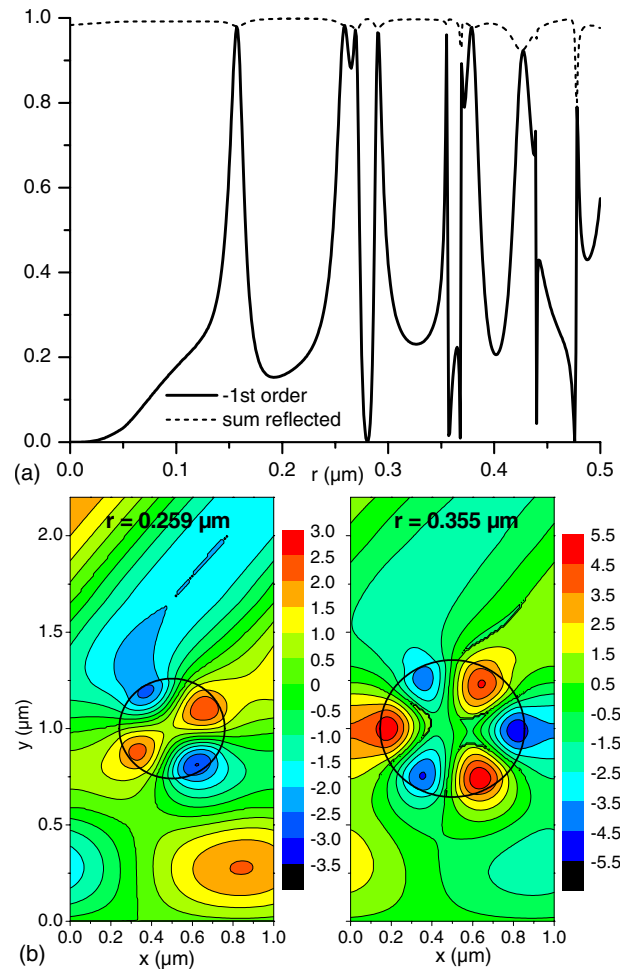


Fig. 8. (Color online) (a) Efficiency in order  $-1$  and the sum of orders  $-1$  and  $0$  for a grating with  $n_1=1.5$  as given in Fig. 7(a) with  $h=0.010 \mu\text{m}$  and other parameters as in Fig. 5. (b) Electric field map for two different radii and the other parameters described in (a).

$c=0.3 \mu\text{m}$ . As can be expected, the wider rods show greater number of resonances than the narrower ones.

Similar dielectric lamellar gratings have been proposed for different purposes. 25 years ago Yokomori showed the possibility to obtain perfect blazing in transmission [26]. More recently, such systems were used for beam-splitting in laser cavity [27]. Perfect blazing in reflection was obtained in [28], which was explained by the authors with the excitation of a leaky wave inside the dielectric system. We are more convinced to conclude that in our case it is not necessary to introduce leaky waves, because the interference between the propagating orders is sufficient, as shown in Section 3. Moreover, a blazing in reflection similar to the one observed in Fig. 1 is observed in normal incidence on dielectric structures having rectangular cross-sections and resulting either from the excitation of leaky guided modes or from purely propagating waves [29–33].

As an additional argument to confirm the role of the propagating waves in our case, the dependence of the efficiency on the non-corrugated layer thickness shows a periodic variation [Fig. 9(b)] typical of Fabry–Perot resonances obtained with propagating waves. It is sufficient to have electromagnetic resonances in order to obtain perfect blazing, as discussed in Section 3.

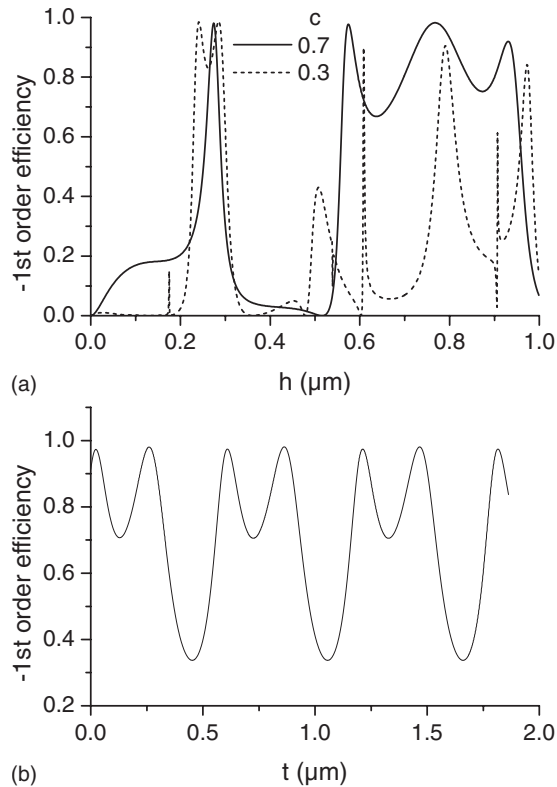


Fig. 9. (a) Diffraction efficiency in the  $-1$ st order for the system sketched in Fig. 7(c) as a function of the rod height  $h$  for two different widths,  $d = 1 \mu\text{m}$ ,  $\lambda = 1.55 \mu\text{m}$ ,  $\theta_i = 50.8^\circ$ ,  $n_1 = 1.5$ , substrate is gold, rod index is 3.45, and the rod center is kept at a constant height  $H = t + h/2$  of  $1 \mu\text{m}$  from the substrate. The solid curve is for  $c = 0.7 \mu\text{m}$  (rod width of  $0.3 \mu\text{m}$ ); the dashed curve is for  $c = 0.3 \mu\text{m}$ . (b) The same as in (a) but as a function of the distance  $H$  between the rod center and the metallic substrate for almost square rod with width of  $0.3 \mu\text{m}$  ( $c = 0.7 \mu\text{m}$ ) and  $h = 0.274 \mu\text{m}$ .

Figure 10 shows the electric field maps corresponding to the first maximum in Fig. 9(a) with  $c = 0.7 \mu\text{m}$  and  $h = 0.274 \mu\text{m}$ , with and without the metallic substrate. In

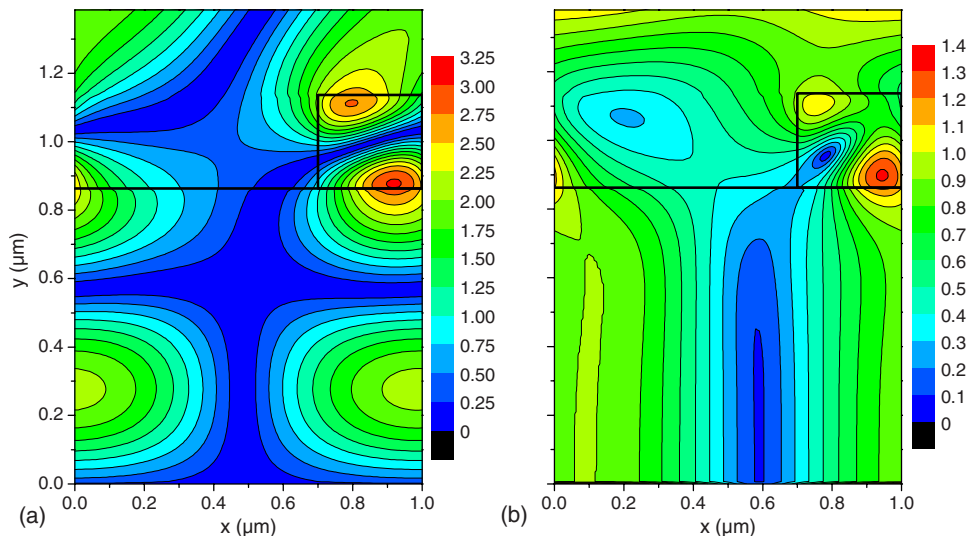


Fig. 10. (Color online) Map of  $|E|$  in the case with a metallic gold substrate (on the left) or with a substrate having the same index as the lower layer (on the right). The system is sketched in Fig. 7(c) with  $d = 1 \mu\text{m}$ ,  $c = 0.7 \mu\text{m}$ ,  $h = 0.274 \mu\text{m}$ , refractive index of the rod is 3.45,  $n_1 = 1.5$ ,  $t = 0.863 \mu\text{m}$ ,  $\lambda = 1.55 \mu\text{m}$ , and  $\theta_i = 50.8^\circ$ . The heavy lines present the boundaries of the different media.

both cases there is clearly visible field enhancement inside the high-index rods, although it is lower than in the case of circular rods. With the metallic substrate, we observe maxima in the lower layer due to the interference between the four waves that propagate inside, while without the reflecting substrate there is an interference pattern due to the two diffracted orders in transmission: the zeroth one propagating to the right with an efficiency of 33% and the  $-1$ st one propagating to the left with an efficiency of 50%

The importance of these effects for practical application appears even more clearly when realizing that the resonances responsible for the high efficiency are located far from the metallic surface and that the interaction between the diffractive system and the metal happens mainly through propagating waves, which prevents the resonance increase of absorption losses. Another consequence of the general conclusions of Section 3 is that the perfect blazing can be expected whatever the incident angle and the polarization may be. We have already presented in Section 3 an example with a fiber grating working in grazing incidence ( $75^\circ$ ) and showing perfect blazing in TE polarization, a property that has been limited to diffractive echelles. Figure 11 presents the diffraction efficiency for a rectangular rod grating as a function of the bump height  $h$  for two mountings, different from the mounting in Fig. 9. Littrow mount with incident and diffracted angles equal to  $75^\circ$  corresponds to Fig. 11(a) that demonstrates the possibility to obtain perfect blazing (vanishing specular reflection) in TE and transverse magnetic (TM) polarizations. Another interesting mount with grazing incidence but diffraction at a smaller angle can be used for beam expanding, and it is almost impossible with known gratings to obtain a high efficiency. Figure 11(b) demonstrates this possibility for both polarizations. In fact, it is possible to generalize the considerations of Section 3 to non-Littrow mount and to obtain the same conclusions that the zeros of the scattering matrix compo-

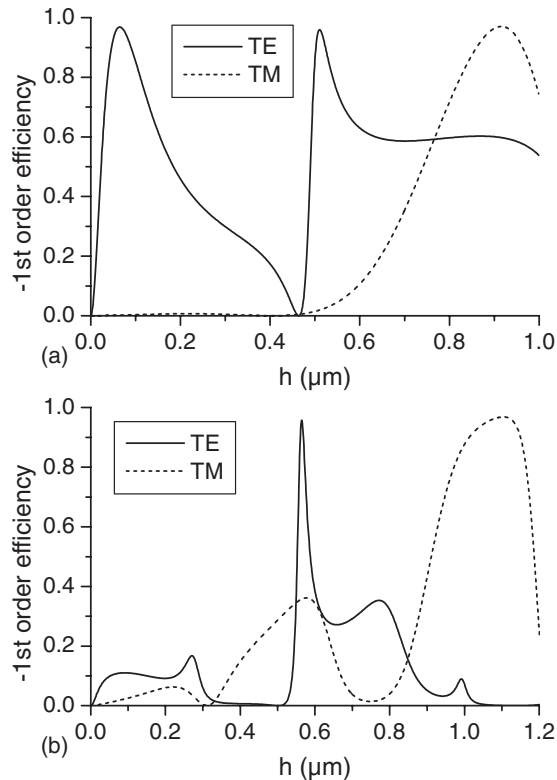


Fig. 11. (a) Diffraction efficiency in the  $-1$ st order in grazing Littrow mount for the system sketched in Fig. 7(c) as a function of the rod height  $h$ ,  $d=0.80234 \mu\text{m}$ ,  $c=0.7 \mu\text{m}$ ,  $\lambda=1.55 \mu\text{m}$ ,  $\theta_i=75^\circ$ ,  $n_1=1.5$ , substrate is gold, rod index is 3.45, and the rod center is kept at a constant height  $H=t+h/2$  of  $1 \mu\text{m}$  from the substrate. The solid curve is for TE polarization; the dashed curve is for TM polarization. (b) The same as in (a), but with period  $d=1 \mu\text{m}$  so that the diffraction direction is at  $35^\circ$ .

nents are real in order to explain the perfect blazed observed in Fig. 11(b).

## 6. CONCLUSIONS

Combining cavity or whispering gallery mode resonances and interference effects between a grating structure and a plane metallic substrate can lead to perfect blazing in Littrow or off-Littrow mount, and also close to grazing incidence even if the grating is not blazed. The fact that the electromagnetic field enhancement appears far from the metal surface reduces significantly the absorption losses, and thus the absolute diffraction efficiency can exceed 99%.

## REFERENCES

1. Th. Young, "On the theory of light and colors," *Philos. Trans. R. Soc. London* **2**, 399–408 (1803).
2. F. Hopkinson and D. Rittenhouse, "An optical problem, proposed by Mr. Hopkinson, and solved by Mr. Rittenhouse," *Trans. Am. Phil. Soc.* **2**, 201–206 (1786).
3. E. Loewen and E. Popov, *Diffraction Gratings and Applications* (Marcel Dekker, 1997).
4. D. Maystre, "Photonic crystal diffraction gratings," *Opt. Express* **8**, 209–216 (2001).
5. E. Popov, B. Bozhkov, and M. Nevière, "Almost perfect blazing by photonic crystal rod gratings," *Appl. Opt.* **40**, 2417–2422 (2001).

6. E. Popov, L. Mashev, and D. Maystre, "Theoretical study of the anomalies of coated dielectric gratings," *Opt. Acta* **33**, 607–619 (1986).
7. F. Lemarchand, A. Sentenac, and H. Giovannini, "Increasing the angular tolerance of resonant grating filters with doubly periodic structures," *Opt. Lett.* **23**, 1149–1151 (1998).
8. A.-L. Fehrembach, E. Popov, G. Tayeb, and D. Maystre, "Narrow-band filtering with whispering modes in gratings made of fibers," *Opt. Express* **15**, 15734–15740 (2007).
9. Lord Rayleigh, "Whispering gallery modes," *Philos. Mag.* **20**, 1001–1004 (1910).
10. Lord Rayleigh, "The problem of the whispering gallery," in *Scientific Papers* (Cambridge U. Press, 1912), Vol. 5, pp. 617–620.
11. H. Mahlein, "Fibre-optic communication in the wavelength-division multiplex mode," *Fiber Integr. Opt.* **4**, 339–372 (1983).
12. C. M. deBolk and P. Mathiesse, "Core alignment procedure for single-mode-fibre jointing," *Electron. Lett.* **20**, 109–110 (1984).
13. R. Morgan, J. S. Barton, P. G. Harper, and J. D. C. Jones, "Wavelength dependence of bending loss in monomode optical fibers: effect of the fiber buffer coating," *Opt. Lett.* **15**, 947–949 (1990).
14. F. M. Haran, J. S. Barton, and J. D. C. Jones, "Determination of monomode fiber buffer properties from bend-loss measurements," *Opt. Lett.* **18**, 1618–1620 (1993).
15. R. D. Morgan, J. D. C. Jones, J. S. Barton, and P. G. Harper, "Determination of monomode fiber buffer properties," *J. Lightwave Technol.* **12**, 1355–1359 (1994).
16. F. M. Haran, J. S. Barton, S. R. Kidd, and J. D. C. Jones, "Optical-fiber interferometric sensors using buffer guided light," *Meas. Sci. Technol.* **5**, 526–530 (1994).
17. F. M. Haran, J. S. Barton, and J. D. C. Jones, "Bend loss in buffered over-moded optical-fiber—lp(11) mode and whispering-gallery mode interaction," *Electron. Lett.* **30**, 1433–1434 (1994).
18. Y. Powell-Friend, L. Phillips, T. George, and A. Sharma, "A simple technique for investigating whispering gallery modes in optical fibers," *Rev. Sci. Instrum.* **69**, 2868–2870 (1998).
19. S. Olivier, C. Smith, M. Rattier, H. Benisty, C. Weisbuch, T. Krauss, R. Houdre, and U. Oesterle, "Miniband transmission in a photonic crystal coupled-resonator optical waveguide," *Opt. Lett.* **26**, 1019–1021 (2001).
20. T. D. Happ, M. Kamp, A. Forchel, J.-L. Gentner, and L. Goldstein, "Two-dimensional photonic crystal coupled-defect laser diode," *Appl. Phys. Lett.* **82**, 4–6 (2003).
21. A. D. Bristow, D. M. Whittaker, V. N. Astratov, M. S. Skolnick, A. Tahraoui, T. F. Krauss, M. Hopkinson, M. P. Groucher, and G. A. Gehring, "Defect states and commensurability in dual-period  $\text{Al}_x\text{Ga}_{1-x}\text{As}$  photonic crystal waveguides," *Phys. Rev. B* **68**, 033303 (2003).
22. S. Deng, W. Cai, and V. Astratov, "Numerical study of light propagation via whispering gallery modes in microcylinder coupled resonator optical waveguides," *Opt. Express* **12**, 6468–6480 (2004).
23. D. Felbacq, G. Tayeb, and D. Maystre, "Scattering by a random set of parallel cylinders," *J. Opt. Soc. Am. A* **11**, 2526–2538 (1994).
24. E. Popov and M. Nevière, "Maxwell equations in Fourier space: fast converging formulation for diffraction by arbitrary shaped, periodic, anisotropic media," *J. Opt. Soc. Am. A* **18**, 2886–2894 (2001).
25. D. Maystre, "Integral methods," in *Electromagnetic Theory of Gratings*, R. Petit, ed. (Springer-Verlag, 1980), Chap. 3.
26. K. Yokomori, "Dielectric surface relief gratings with high diffraction efficiency," *Appl. Opt.* **23**, 2303–2310 (1984).
27. M. Merimaa, H. Talvitie, P. Laakkonen, M. Kuittinen, I. Tittonen, and E. Ikonen, "Compact external-cavity diode laser with a novel transmission geometry," *Opt. Commun.* **174**, 175–180 (2000).
28. N. Destouches, A. Tishchenko, J. Pommier, S. Reynaud, O. Parriaux, S. Tonchev, and M. Ahmed, "99% efficiency mea-

- sured in the  $-1$ st order of a resonant grating,” *Opt. Express* **13**, 3230–3235 (2005).
29. C. F. R. Mateus, M. C. Y. Huang, Y. Deng, A. R. Neureuther, and C. J. Chang-Hasnain, “Ultrabroadband mirror using low-index cladded subwavelength grating,” *IEEE Photon. Technol. Lett.* **16**, 518–520 (2004).
  30. Ph. Lalanne, J. P. Hugonin, and P. Chavel, “Optical properties of deep lamellar gratings: a coupled Bloch-mode insight,” *J. Lightwave Technol.* **24**, 2442–2449 (2006).
  31. L. Chen, M. C. Y. Huang, C. F. R. Mateus, C. J. Chang-Hasnain, and Y. Suzuki, “Fabrication and design of an integrable subwavelength ultrabroadband dielectric mirror,” *Appl. Phys. Lett.* **88**, 031102 (2006).
  32. M. Shokooh-Saremi and R. Magnusson, “Wideband leaky-mode resonance reflectors: influence of grating profile and sublayers,” *Opt. Express* **16**, 18249–18263 (2008).
  33. R. Magnusson and M. Shokooh-Saremi, “Physical basis for wideband resonant reflectors,” *Opt. Express* **16**, 3456–3462 (2008).